ELSEVIER

MCN Molecular and Cellular Neuroscience

www.elsevier.com/locate/ymcne
Mol. Cell. Neurosci. 32 (2006) 283 – 298

The effects of a dominant connexin32 mutant in myelinating Schwann cells

Linda Jo Bone Jeng,[a,1] Rita J. Balice-Gordon,[b] Albee Messing,[c] Kenneth H. Fischbeck,[d,2] and Steven S. Scherer[d,*]

[a] *Cell and Molecular Biology Graduate Group, The University of Pennsylvania Medical Center, Philadelphia, PA 19104-6077, USA*
[b] *Department of Neuroscience, The University of Pennsylvania Medical Center, Philadelphia, PA 19104-6077, USA*
[c] *Department of Pathobiological Sciences, School of Veterinary Medicine, University of Wisconsin-Madison, Madison, WI 53706, USA*
[d] *Department of Neurology, The University of Pennsylvania Medical Center, 464 Stemmler Hall, 36th Street and Hamilton Walk, The University of Pennsylvania Medical Center, Philadelphia, PA 19104-6077, USA*

Received 20 December 2005; revised 25 April 2006; accepted 1 May 2006

Mutations in *GJB1*, the gene encoding the gap junction protein connexin32 (Cx32), cause X-linked Charcot–Marie–Tooth disease, an inherited demyelinating peripheral neuropathy. We generated transgenic mice that express the R142W mutation in myelinating Schwann cells. The R142W mutant protein was aberrantly localized to the Golgi, indicating that it does not traffic properly, but the molecular organization of the myelin sheath, including the localization of Cx29, another connexin expressed by myelinating Schwann cells, was not disrupted. In a wild type background, this mutation dramatically decreased the level of wild type mouse Cx32 in immunoblots of sciatic nerve and caused demyelination. The expression of wild type human Cx32 with the same transgenic construct had different effects—increased amounts of Cx32, normal localization of Cx32 at nodes and incisures, and split myelin sheaths. Thus, the R142W mutant protein has dominant effects that are distinct from overexpression.

Keywords: Charcot–Marie–Tooth disease; CMT1X; Gap junctions; Neuropathy; Protein trafficking

Introduction

Charcot–Marie–Tooth disease (CMT) is a genetically heterogeneous group of non-syndromic inherited neuropathies, with shared clinical features of slowly progressive weakness, atrophy, and sensory loss in the distal extremities (Lupski and Garcia, 2001; Wrabetz et al., 2004; Shy et al., 2005). The dominantly inherited demyelinating forms, CMT1, typically have slower nerve conduction velocities than do the dominantly inherited axonal/neuronal forms (CMT2). Segmental demyelination and remyelination are the primary pathological changes in CMT1, but there is axonal loss over time. Mutations in the *PMP22*, *MPZ/P0*, *LITAF/SIMPLE*, *EGR2*, and *GJB1/Cx32* cause CMT1. Myelinating Schwann cells express all of these genes, several of which encode intrinsic membrane proteins of the myelin sheath—PMP22, P_0, and connexin32 (Cx32). Cx32 is a member of a family of highly homologous proteins, the connexins (Bruzzone et al., 1996), six of which form a hemi-channel or connexon. Tightly apposed hemi-channels on adjacent cell membranes form channels that allow the passage of ions and molecules less than 1000 Da. Cx32 is localized to incisures and paranodes, regions of non-compact myelin, and probably forms gap junctions at these locations (Balice-Gordon et al., 1998; Meier et al., 2004).

More than 270 different *GJB1* mutations cause CMT1X (http://www.molgen.ua.ac.be/CMTMutations/Datasource/mutbygene.cfm). These mutations affect all regions of human Cx32 protein (hCx32). All mutations appear to cause CMT1X; no polymorphic amino acid substitutions have been described. Furthermore, many hCx32 mutants cause a loss of function in electrophysiological assays (Abrams et al., 2000; Abrams et al., 2001; Wang et al., 2004); most of these do not reach the cell membrane in transfected mammalian cells, appearing to be retained in the endoplasmic reticulum (ER) or Golgi (Yum et al., 2002). A loss of function is sufficient to cause demyelination as deletion of the *GJB1/Gjb1* gene in humans/mice causes a demyelinating neuropathy (Anzini et al., 1997; Ainsworth et al., 1998; Scherer et al., 1998), demonstrating that human and mouse Cx32 (mCx32) have an essential function in myelinating Schwann cells. Some *GJB1* mutations, however, have additional deleterious effects. In particular, several mutations (R75W, E102deleted, R142W,

* Corresponding author. Fax: +1 215 573 4454.
E-mail address: sscherer@mail.med.upenn.edu (S.S. Scherer).
[1] Current address: Department of Genetics and Center for Human Genetics, University Hospitals of Cleveland and Case Western Reserve University, Cleveland, OH 44106, USA.
[2] Current address: Neurogenetics Branch, Neurogenetics Branch, NINDS, NIH, 35-2A1000, 35 Convent Dr., MSC 3705, Bethesda, MD 20892-3705, USA.

Available online on ScienceDirect (www.sciencedirect.com).

1044-7431/$ - see front matter © 2006 Elsevier Inc. All rights reserved.
doi:10.1016/j.mcn.2006.05.001

R164W, C168Y) appear to cause transient episodes of CNS dysfunction associated with reversible abnormalities in the white matter of the brain (Taylor et al., 2003). We generated transgenic (TG^+) mice expressing R142W, a missense mutation that replaces arginine with tryptophan at position 142 in the third transmembrane domain. All family members with this mutation, both males and females, are symptomatic (originally described as family 243; (Bergoffen et al., 1993). In *Xenopus* oocytes, the R142W mutant does not form functional gap junctions and has a pronounced dominant negative effect when co-expressed with either wild type (WT) Cx26 or Cx32 (Bruzzone et al., 1994). In TG^+ mice, the R142W mutant is localized to the Golgi in myelinating Schwann cells, reduces the level of endogenous mCx32, and causes demyelination. These results suggest that some Cx32 mutants can have dominant-negative interactions and that disease mechanisms other than a simple loss of function play a role in the pathogenesis of CMT1X (Liang et al., 2005).

Results

Generation of Cx32 transgenic mice

Transgenic constructs designed to express WT hCx32, the R142W mutation, and the R142W mutation with a C-terminal HA tag were designated P0Cx32WT, P0243, and P0243HA, respectively (Fig. 1A). A 1.1 kb fragment containing the rat *Mpz* promoter (Lemke et al., 1988), which drives expression in myelinating Schwann cells in TG^+ mice (Messing et al., 1992), was cloned to the *GJB1* gene. Because transgenes made with genomic DNA are expressed at higher levels than those made with cDNA (Brinster et al., 1988; Palmiter et al., 1991), we used the human *GJB1/Cx32* genomic fragment containing exons 1b and 2 and the intervening intron. Other derivates of this *Mpz-GJB1* construct successfully drive the expression of transgenes in myelinating Schwann cells (Abel et al., 1999; Pot et al., 2002; Leone et al., 2003; Scherer et al., 2005). Pronuclear injection of isolated transgene cassettes into fertilized oocytes resulted in the generation of three P0243HA founders (6, 10, and 17), five P0243 founders (153, 157, 165, 167, and 179), and ten P0Cx32WT founders (73, 77, 88, 90, 93, 94, 96, 103, 104, and 110). All founders were able to establish transgenic lines. No obvious behavioral abnormalities were observed in these founders or their offspring, for up to 8 months for most lines and up to 1 year for line 6.

Expression of transgenic and endogenous Cx32 mRNA

To determine whether the transgene mRNA was expressed in peripheral nerve, we performed RT-PCR on peripheral nerves of single animals with transgene-specific primers (<P0> and <2> in Fig. 1B). RT-PCR amplified a 517 bp product, predicted to be the RNA-specific product, without any amplification of genomic DNA (predicted to be a 872 bp product) from each cDNA sample (data not shown). The amplification of a 553 bp product from the same cDNA samples with primers that recognize common nucleotide sequences (<1> and <4> in Fig. 1B) that are identical in both human and mouse *GJB1/Gjb1*, followed by restriction digestion, allowed us to determine the relative amount of transgenic/human Cx32 mRNA compared to endogenous/mouse Cx32 mRNA (Fig. 1C). *Hha*I uniquely cut the mouse product, while *Msc*I uniquely cut the human product. Densitometric analysis of mouse- and human-specific bands within a single lane showed more than 3-fold higher levels of transgenic/human Cx32 mRNA compared to endogenous/mouse Cx32 cDNA for lines 6 and 157. As previously reported, line 90 had approximately equal levels of transgene and endogenous Cx32 cDNA, whereas line 96 had 3-fold higher levels

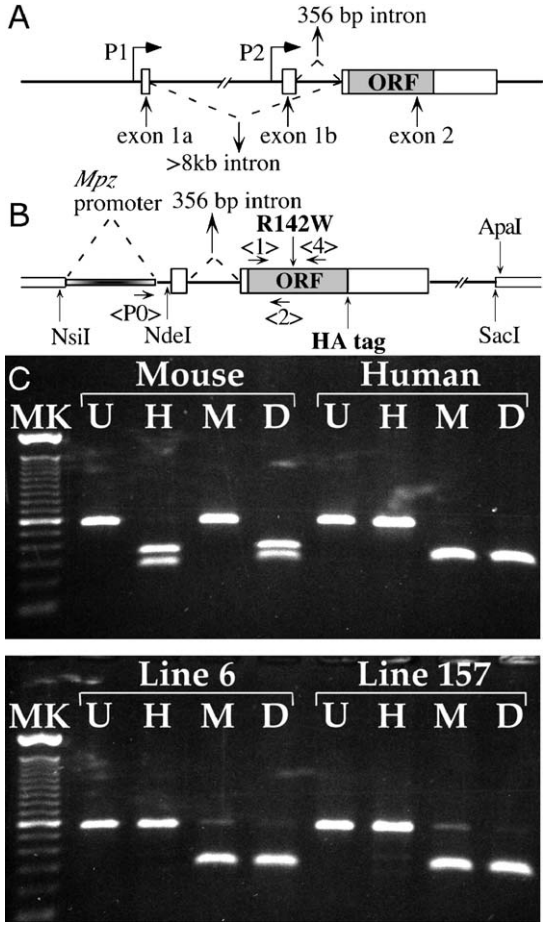

Fig. 1. Generation and RT-PCR analysis of *GJB1* TG^+ mice. (A) Schematic structure of the *GJB1* gene. Lines depict introns and boxes depict exons; the open portions depict untranslated regions; the gray portion depicts the open reading frame (ORF), which is contained within the second exon and is included in transcripts initiated at either the P1 or the P2 promoters. (B) Schematic map of the *Mpz-GJB1* transgene constructs. The 5.3 kb *Nde*I/*Sac*I fragment of *GJB1* was cloned 3′ to the 1.1 kb rat *Mpz* promoter fragment. *Nde*I cuts 7 bp 3′ the P2 promoter TATAA box, which is thus excluded from the transgene construct. Flanking vector sequences are shown as open-ended boxes on either side of the construct. The transgene cassette is isolated by a *Nsi*I and *Apa*I double digest. Primers used for PCR genotyping and RT-PCR analysis are indicated as <P0>, <1>, <2>, and <4>. The R142W mutation and HA tag insertion sites are marked. (C) Analysis of endogenous versus transgene expression by RT-PCR. The top panel (Scherer et al., 2005) shows human/mouse *GJB1/Gjb1* cDNA amplified with primers (<1> and <4>) that hybridize with a sequence that is identical in human and mouse *GJB1/Gjb1*. The undigested (U) PCR product is 553 bp; *Hha*I (H) cuts mouse but not human Cx32 cDNA, *Msc*I (M) cuts human but not mouse Cx32 cDNA; the double digestion (D) proves that no full-length product remains. The bottom panel shows similarly digested RT-PCR products from adult TG^+ sciatic nerve. Densitometric quantitation of the human- and mouse-specific bands in the *Msc*I cut lane indicates that the ratio of hCx32/mCx32 cDNA is 8 and 10 for lines 6 and 157, respectively. MK: DNA size markers.

of transgenic/human Cx32 cDNA (Scherer et al., 2005). These experiments were performed on two animals from each line (4 and 8 weeks old for TG^+ mice expressing R142W or R142W-HA, and 5 and 25 weeks old for TG^+ mice expressing WT hCx32), with the same results.

Immunoblot analysis of transgenic/human Cx32 protein

Antibodies do not distinguish between mCx32 and hCx32 because they are nearly identical, so that immunoblotting sciatic nerves in TG^+ mice in a WT background represent the sum of the endogenous/mouse and transgenic/human Cx32. Transgenic lines expressing P0Cx32 (WT hCx32) had increased levels of Cx32 protein compared to normal mice (Fig. 2A)–line 90 had the smallest increase, and lines 77 and 96 had much higher levels–regardless of whether the nerves were taken from juvenile (1–2 months old, before demyelination was present) or adult mice (4–6 months old, after demyelination was evident). The increased levels of Cx32 indicate that the transgenic/human Cx32 is expressed, which we have directly demonstrated by immunoblot analysis of nerves from TG^+ male mice from lines 90 and 96 (WT hCx32) in a *Gjb1/cx32*-null background (Scherer et al., 2005). Thus, P0Cx32WT lines have increased levels of Cx32 mRNA and protein, resulting from the expression of the transgene.

In contrast to P0Cx32WT lines, the sciatic nerves in two of three P0243HA (R142W-HA) lines (6 and 17) and three of five P0243 (non-HA-tagged) lines (153, 157, and 165) had *lower* levels of Cx32 than did nerves from WT mice (Fig. 2A). The decreased levels of Cx32 were not the result of unequal loading or less myelin protein as the Coomassie-stained gel showed similar levels of P_0 protein. Similar results were found with a different antibody against Cx32 (Fig. 2C), and using nerves from young and old animals (data not shown). Furthermore, immunoblot analysis demonstrated that the levels of myelin basic protein (MBP) and

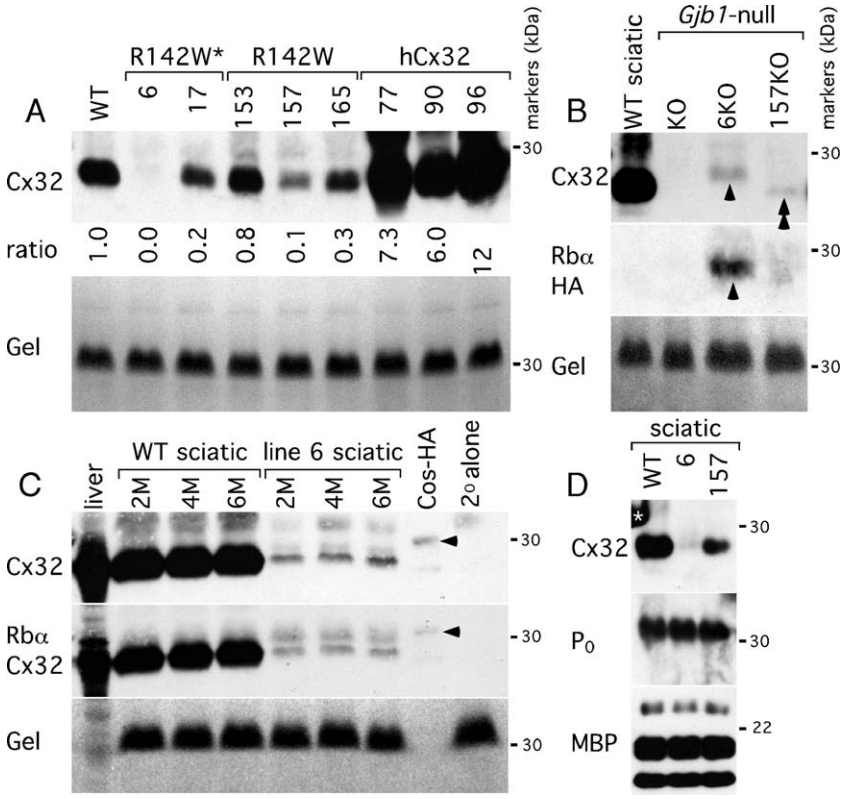

Fig. 2. Immunoblot analysis of transgenic mice. Each panel shows scanned images of immunoblots for the indicated proteins and/or the Coomassie-stained gels after transfer (gel); samples are from individual mice except where indicated. A mouse monoclonal antibody (7C6.C7) was used to visualize Cx32, except where noted (panel C). P_0 is the prominent (32 kDa) band in the gels. (A) Cx32 expression in sciatic nerves from wild type mice (WT) as well as lines expressing HA-tagged R142W (R142W*; 6 and 17), untagged R142W (153, 157, and 165), or WT hCx32 (77, 90, and 96), all in a WT mouse background. For each lane, the amount of Cx32 and P_0 was measured by densitometry and is shown as a ratio relative to that for WT nerves (arbitrarily set at 1.0). A longer exposure of the blot than the one shown here was used to demonstrate Cx32 for line 6. (B) Transgenic/human Cx32 expression in sciatic nerves in the absence of endogenous/mouse Cx32. Note the low levels of hCx32 in lines 6KO (R142W-HA) and 157KO (R142W) compared to that in WT mouse nerve, and the absence of any band in *Gjb1/cx32*-null nerve (KO). R142W-HA (arrowhead) is relatively larger than untagged R142W (double arrowheads); the identity of the larger band (arrowhead) as R142W-HA was confirmed by rehybridizing the blot with a rabbit antiserum against HA. (C) Extracts from WT and line 6 (two different mice) sciatic nerves (R142W-HA) treated with 2, 4, or 6 M urea to diminish protein aggregates, along with extracts of normal mouse liver and Cos cells transfected to express WT hCx32-HA. The blot was rehybridized with a rabbit antiserum against Cx32 (Zymed). Both hybridizations show that the levels of Cx32 are lower in line 6 than in WT nerves. Note that the rabbit antiserum labels two discrete bands of Cx32 immunoreactivity in line 6 sciatic nerves and that WT hCx32-HA expressed by transfected Cos cells (arrowheads) runs about the same size as the upper band. No signal is seen in a sample from WT mouse sciatic nerve hybridized with secondary antibody alone (2° alone). (D) Extracts of sciatic nerves from WT mice, as well as from line 6 (R142W-HA), and line 157 (R142W) in a WT background, probed for Cx32, P_0, and MBP. Note that nerves from lines 6 and 157 contain lower levels of Cx32, but similar levels of P_0 and MBP. The asterisk marks the signal from hybridization to the 30 kDa size marker.

P_0 were not affected in these transgenic lines (Fig. 2D). To evaluate further the apparent decrease of endogenous Cx32 in mutant nerves, we looked for protein aggregates in the stacking gel (data not shown), treated samples with urea to break aggregates (Fig. 2C), ran short gels to look for small degradation products (data not shown), and treated nerve explants with chloroquine overnight at 37°C (data not shown) to block the lysosomal degradation pathway (Notterpek et al., 1997). None of these approaches resulted in the identification of additional Cx32 protein or degradation products. While we favor the idea that increased degradation causes the lower level of mutant protein, we have not ruled out the possibility that decreased transcription or stability of its mRNA and/or decreased detection of the mutant protein (caused by misfolding, for example) are contributing factors. These results indicate that expression of the R142W mutant, but not WT hCx32, interferes with the expression or processing of endogenous mCx32, but not of other myelin proteins.

In a WT background, immunoblots of nerves from line 6 (R142W-HA) often had two discrete bands, as shown in Fig. 2C. It seemed plausible that the larger band was R142W-HA, and the smaller band was WT mCx32, as we detected a similar size difference between HA-tagged and non-tagged hCx32 in transiently transfected Cos cells (Fig. 2C). To analyze this issue, we generated TG^+ male mice in a *Gjb1* knockout (KO) background by breeding male TG^+ animals from lines 6 and 157 with *Gjb1*-null females. In the male offspring that were TG^+ (termed 6KO and 157KO), all of the Cx32 protein was derived from the transgene. In Fig. 2B, note that immunoblots of sciatic nerves from 6KO and 157KO males had markedly decreased levels of Cx32 compared to WT nerves, that the Cx32 in 6KO nerves was larger than that in line 157KO nerves, that an antiserum against HA recognized this larger band in 6KO nerves (but not the smaller band in 157KO nerves), and that *Gjb1*-null nerves lacked both bands. These data, taken together, demonstrate that, although transgenic/human Cx32 mRNA is expressed at higher levels than endogenous/mouse Cx32 mRNA, both the R142W and R142W-HA proteins are found at lower levels than the WT hCx32 protein, indicating that the mutant protein does not accumulate comparably. Furthermore, in a WT mouse background, the mutant hCx32 dramatically reduces the levels of the endogenous mCx32, an effect that was not seen in liver (data not shown), a tissue that expresses Cx32 but that does not express the *Mpz-GJB1* transgene (Scherer et al., 2005).

Localization of transgenic/human Cx32

To localize Cx32, unfixed teased fibers from adult mice from lines 77, 90, and 96 (expressing WT hCx32) were immunostained with monoclonal antibodies (7C6.C7 or M12.13) or rabbit antisera against Cx32 (one from Chemicon and another from Dr. David Paul). All these antibodies labeled incisures and paranodes in WT mice (Fig. 3A, and data not shown), but not in *Gjb1*-null mice (data not shown; Scherer et al., 1998; Scherer et al., 2005). In a WT background, Cx32 immunoreactivity was predominantly found in incisures and paranodes of TG^+ mice (Figs. 3B and C), but in lines 77, 90, and 96, the amount of Cx32 was increased, with large aggregates not seen in WT nerves, similar to what we found for lines 90 and 96 TG^+ mice in a *Gjb1*-null background (Scherer et al., 2005). In either a WT or a KO background, Cx32 immunoreactivity did not accumulate in the perinuclear region, and the ultrastructure of the ER and Golgi was normal; they were not dilated and there was no retained material (Supplemental Fig. 1). As in a *Gjb1*-null background (Scherer et al., 2005), the expression of WT hCx32 did not alter the localization of Cx29 (Fig. 4), another connexin expressed by myelinating Schwann cells (Altevogt et al., 2002). Furthermore, the localizations of E-cadherin (Supplemental Fig. 2) and claudin-19 (Supplemental Fig. 3), components of adherens and tight junctions, respectively (Fannon et al., 1995; Miyamoto et al., 2005), as well as myelin-associated glycoprotein (MAG; Supplemental Fig. 4), were not disrupted. These results demonstrate that, even though it is overexpressed, WT hCx32 protein is properly targeted and does not disrupt the molecular organization of other components of the myelin sheath.

In contrast, immunostaining teased fibers from R142W-HA (lines 6 and 17) and R142W (lines 153, 157, and 165) revealed that Cx32 immunoreactivity was predominately localized to the perinuclear region in a WT background (Figs. 3D–H). These findings were observed in multiple stainings of several animals from each line with the mouse monoclonal against Cx32 and were confirmed with another mouse monoclonal antibody and two different rabbit antisera (data not shown). To investigate the localization of the perinuclear Cx32 staining, we double-labeled teased fibers from lines 6 (Figs. 3G and H) and 157 (data not shown) and found that Cx32 immunoreactivity mainly colocalizes with Golgi markers (58K protein and MG160), although some of the staining extends beyond the Golgi, probably to the ER. We also examined TG^+ male mice in KO background, for both lines 6 (6KO, Figs. 3I and J) and 157 (157KO, data not shown), in which all of the Cx32 was derived from the expression of the transgene. In accord with the above findings, Cx32 immunoreactivity was confined in the perinuclear region; incisures and paranodes were not labeled (Figs. 3I and J). Finally, we immunostained teased fibers from lines 6 and 17 with antibodies against the HA tag (a rat monoclonal and a rabbit antiserum). In both a WT (lines 6 and 17; Figs. 3K and L) and a KO (line 6; Figs. 3I and J) background, these antibodies labeled the perinuclear region, colocalizing with Cx32. These results, taken together, demonstrate that the R142W mutant protein is abnormally localized, and, furthermore, likely causes the mislocalization of endogenous/mouse Cx32. Although R142W was mislocalized, the ultrastructure of the ER and Golgi appeared normal—they were not dilated and there was no accumulation of electron-dense material (Supplemental Fig. 1). Thus, even though the HA tag would be predicted to interrupt the prenylation motif at the C-terminus of Cx32 (Huang et al., 2005), this did not seem to affect its trafficking as compared to non-HA-tagged R142W.

To determine whether the expression of mutant or WT hCx32 affected the localization of other components of the myelin sheath, we immunostained teased fibers in a WT (lines 6, 17, 153, 157, 165, 90, and 96) or KO background (lines 6KO, 153KO, and 157KO) for other components of non-compact myelin. WT and *Gjb1*-null nerves were also labeled. As previously reported for WT and *Gjb1*-null nerves (Altevogt et al., 2002; Li et al., 2002), Cx29 was localized to the incisures, paranodes, and juxtaparanodal region of myelinated axons, although some of the localization shown in Fig. 4 is less than optimal because unfixed, rather than fixed, teased fibers were immunostained. Similarly, the localizations of E-cadherin (Fannon et al., 1995), claudin-19 (Miyamoto et al., 2005), and MAG (Trapp and Quarles, 1982) were not disrupted in *Gjb1*-null (Arroyo et al., 1999) or TG^+ nerves (Supplemental Figs. 2–4). MBP and P_0 were localized to compact myelin (data not shown). No abnormal perinuclear accumulation of Cx29, E-cadherin, claudin-19, MAG, MBP, or P_0 was seen (Fig. 4,

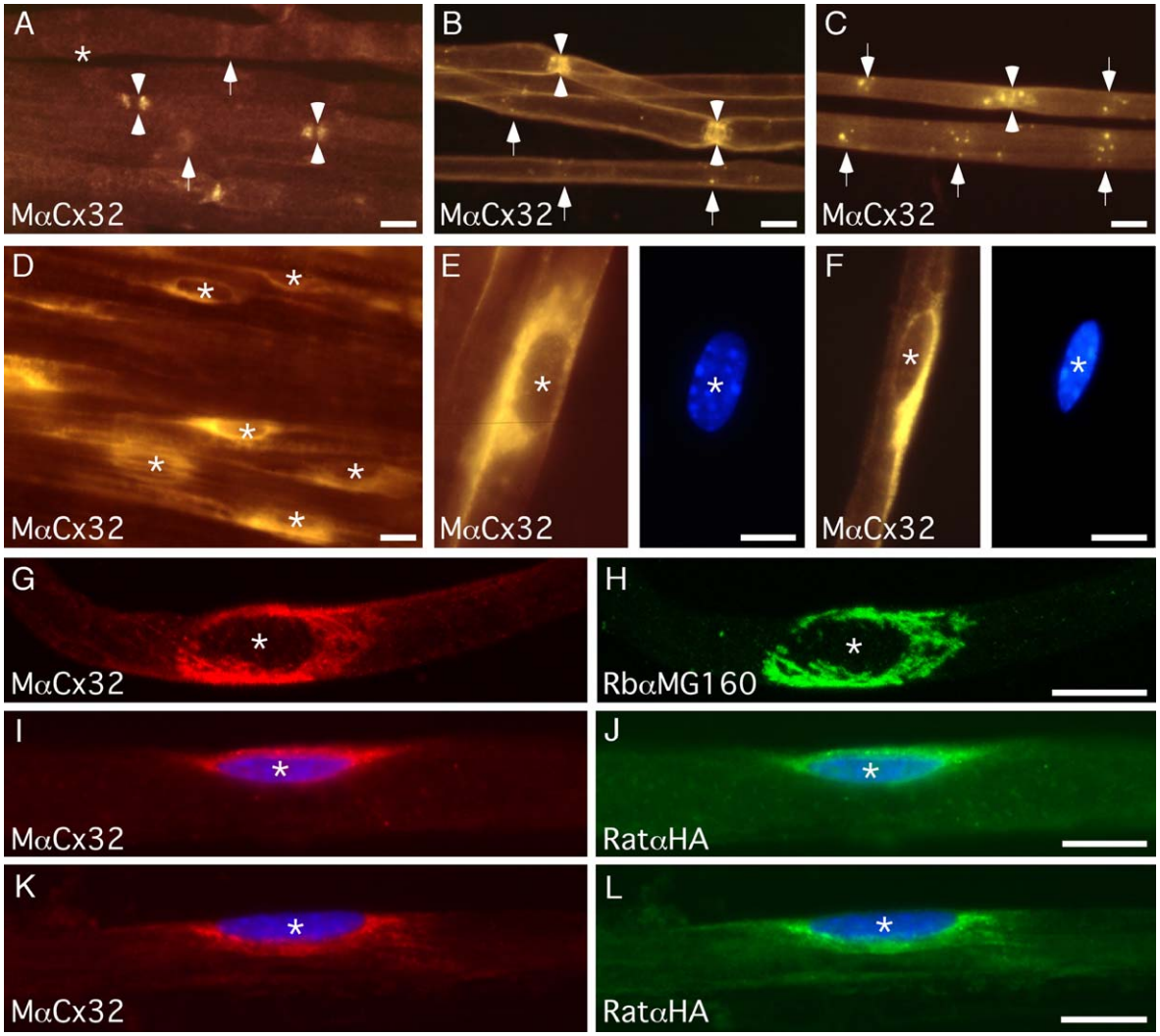

Fig. 3. Localization of R142W (line 157), R142W-HA (line 6) and WT hCx32 (lines 90 and 96). These are images of teased fibers from unfixed adult sciatic nerves, after immunostaining with a monoclonal antibody (7C6.C7; red), a rat monoclonal antibody against hemagglutinin (green), or a rabbit antiserum against a Golgi protein (MG160; green); DAPI was used as a nuclear counterstain (blue). Asterisks mark Schwann cell nuclei, apposed arrowheads mark nodes, and arrows mark incisures. Scale bars: 10 μm. (A) WT mouse. Cx32 immunoreactivity is prominent in paranodes (flanking nodes), and weaker in incisures, and absent in the perinuclear region. (B and C) Lines 90 (B) and 96 (C) in a WT background. Large puncta of Cx32 staining are found chiefly at incisures and paranodes. (D and E) Line 6 in a WT background. Cx32 is localized to the perinuclear region. (F) Line 157 in a WT background. Cx32 is localized to the perinuclear region. (G and H) Line 6 in a WT background, double labeled for Cx32 and MG160, imaged by confocal microscopy. (I and J) Line 6 in a *Gjb1*-null background (6KO), labeled with a mouse monoclonal antibody against Cx32 and a rat monoclonal against HA. Cx32 and HA are colocalized to the perinuclear region. (K and L) Line 6 in a WT background, labeled with a mouse monoclonal antibody against Cx32 and a rat monoclonal against HA. Cx32 and HA are colocalized to the perinuclear region.

Supplemental Figs. 2–4, and data not shown). Thus, the expression of mutant Cx32 did not appear to disrupt the synthesis, trafficking, or localization of other myelin proteins, including another connexin expressed by myelinating Schwann cells.

Functional analysis of gap junctions in the myelin sheaths of Gjb1-null and TG$^+$ mice

Dye transfer studies indicate that incisures contain functional gap junctions (Balice-Gordon et al., 1998). Low molecular mass dyes such as 5,6-carboxyfluorescein (5,6-CF; 376 Da) appear to rapidly diffuse from the outer/abaxonal to the inner/adaxonal cytoplasm via incisures, whereas large molecular mass dyes remained confined to the outer/abaxonal cytoplasm. To determine whether the expression of R142W interrupts this pathway, we injected 5,6-CF into the perinuclear cytoplasm of myelinating Schwann cells of *Gjb1*-null mice and four transgenic lines in a WT background, excluding myelinating Schwann cells with a resting potential more positive than −4 mV. The mean (±SEM) resting potential of the remaining myelinating Schwann cells was similar in each line (−6 ± 3 mV for *Gjb1*-null, $N = 6$; −9 ± 2 mV for line 6, $N = 7$; −8 ± 2 mV for line 157, $N = 6$; −10 ± 4 mV for line 90, $N = 6$; and −7 ± 4 mV for line 96, $N = 9$). Within seconds following the injection, fluorescence was observed in nearby incisures and the cytoplasm on either side of the myelin sheath ("double lines"; Balice-Gordon et al., 1998) for *Gjb1*-null ($N = 6$), line 6 ($N = 7$), line 157 ($N = 6$), line 90 ($N = 5$), and line 96 ($N = 9$). Examples are shown in Fig. 5 for lines 6, 157, and 90. These

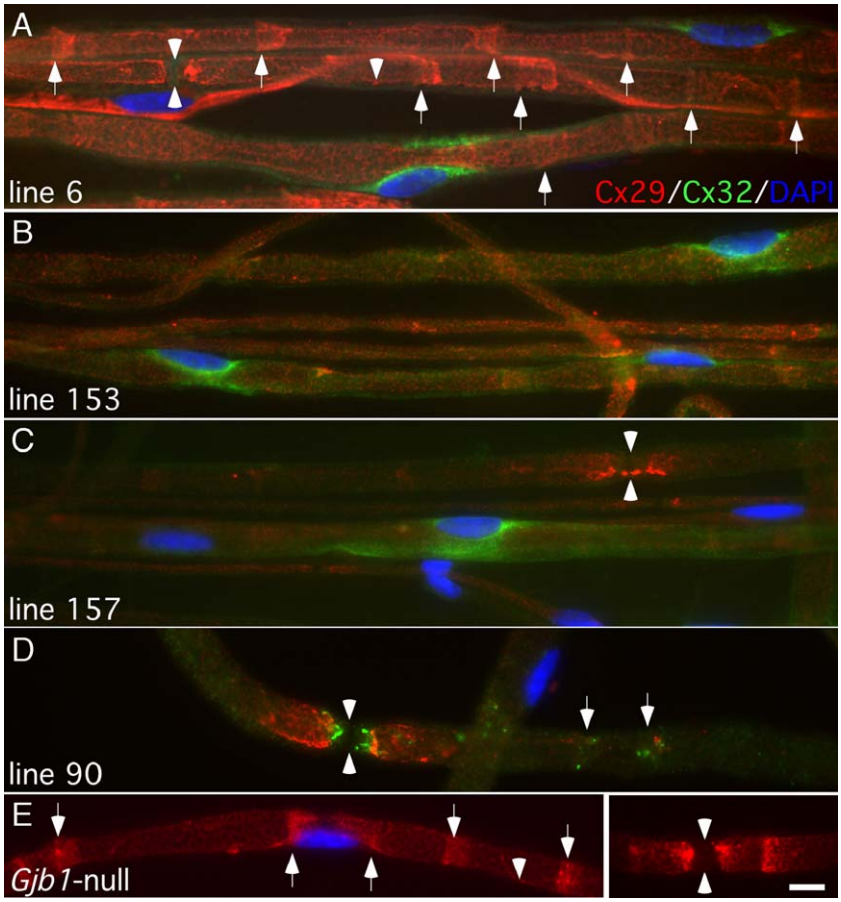

Fig. 4. Normal localization of Cx29 in TG^+ mice. These are images of unfixed teased fibers from TG^+ adult mice that express WT hCx32 (line 90), R142W-HA (line 6), or 142W (lines 153 and 157), all in a WT background, immunostained with mouse and rabbit antibodies against Cx32 and Cx29, respectively, and counterstained with DAPI. In lines expressing R142W or R142W-HA, Cx32 is localized to the perinuclear region. In lines expressing WT hCx32, puncta of Cx32 are found in the paranodal region (flanking nodes) and incisures (arrowheads), but not in the perinuclear region. Cx29 is normally localized in all transgenic lines (A–D) and in *Gjb1*-null mice (E), to incisures (arrows) and juxtaparanodes (flanking nodes; apposed arrowheads), and does not accumulate in the perinuclear region. Scale bars: 10 μm.

results suggest that a gap-junction-mediated pathway still exists within the myelin sheaths of *Gjb1*-null (Balice-Gordon et al., 1998) and TG^+ animals.

Expression of R142W in a WT background causes demyelination

We examined semithin sections of the sciatic nerve, the femoral nerve (which has separate motor and sensory branches), and the dorsal (sensory) and ventral (motor) roots, from mice of varying ages from lines 6, 153, 157, and 165, in a WT background. Together, these samples allowed us to compare the pathological changes in motor versus sensory fibers, as well as proximal versus distal portions of myelinated axons. These results are illustrated in Fig. 6 and Supplemental Figs. 5 and 6 and summarized in Table 1 and Fig. 7A. Few, if any, abnormally myelinated (demyelinated or remyelinated) axons were seen around P100; more were seen at P300—in the motor branch of the femoral nerve (Fig. 6), in fascicles of large (and presumably motor) axons of the sciatic nerve (data not shown), and in the ventral roots (Supplemental Fig. 5) more than in the dorsal roots (data not shown). "Onion bulbs"–concentrically arranged Schwann cell processes surrounding demyelinated or remyelinated axons–were seen in nerves but not in nerve roots. Line 153 was the most affected (Fig. 7A and Table 1), but even in this line the proportion of abnormally myelinated axons was less than seen in age-matched *Gjb1*-null femoral motor branches (Fig. 7A). As in *Gjb1*-null mice (Scherer et al., 1998), demyelinated and remyelinated axons were not seen in the sensory branch of the femoral nerve (the saphenous nerve) in any line at any age (Supplemental Fig. 6). By electron microscopy, the structure of the myelin sheath, including the paranodes and incisures, appeared normal (Supplemental Fig. 1 and data not shown). By comparison, in age-matched, TG^-/WT littermates, remyelinated axons were rarely seen, and demyelinated axons and onion bulbs were not present (Table 1). Thus, mice expressing the R142W transgene had a similar, but much less severe, demyelinating neuropathy than did *Gjb1*-null mice. In line 90 (expresses WT hCx32), there were few demyelinated and remyelinated axons (Table 1), indicating that the expression of transgenic hCx32 alone is not sufficient to cause demyelination.

To confirm the segmental nature of the demyelination, we teased osmicated fibers of the ventral and dorsal roots of the lines expressing R142W or R142W-HA. In the older animals (P200 or more), we found myelin internodes that were immediately adjacent to demyelinated internodes. These demyelinated internodes typically contained extra cells, including supernumerary Schwann cells as well as macrophages containing myelin debris (Fig. 6). In

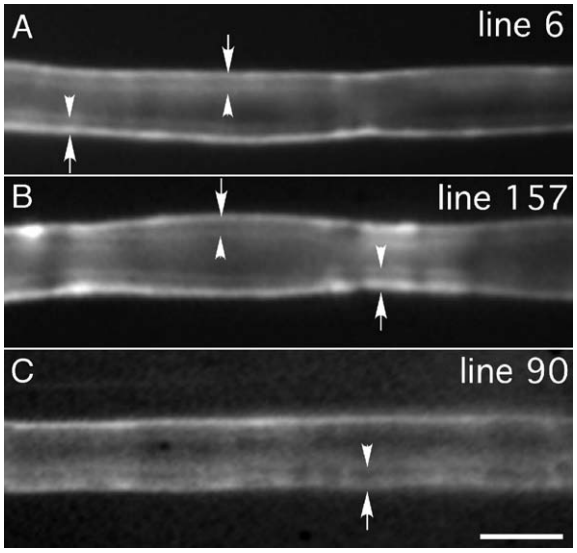

Fig. 5. Functional analysis of gap junctions. Myelinating Schwann cells were injected with 5,6-carboxyfluorescein in the perinuclear region. The diffusion of dye from the outer/abaxonal cytoplasm (arrows) to the inner/adaxonal cytoplasm (arrowheads) is inferred to be mediated by gap junctions within incisures and results in a pair of double lines on either side of the myelin sheath. Examples are shown for lines 6 (R142W-HA), 157 (R142W), and 90 (WT hCx32), all in a WT background. Scale bar: 10 μm.

addition, many well myelinated internodes were apposed to remyelinated internodes (data not shown), recognized by their thinner myelin sheaths and shorter lengths (Dyck et al., 2005). These pathological features were more common in the ventral roots than in the dorsal roots, in keeping with evidence above that these TG^+ mice have an age-related demyelinating neuropathy that predominately affects motor axons. In teased fiber preparations from the TG^-/WT littermates, no demyelinated or remyelinated axons were seen at any age.

To quantitate these findings, we counted all of the demyelinated, remyelinated, and normally myelinated axons in single transverse sections of the femoral motor branch, combining the counts from the left and right sides for individual animals where possible (Fig. 7A and Table 1). This analysis indicated that the proportion of abnormally myelinated (demyelinated and remyelinated) axons increased with age in lines that express R142W or R142W-HA. To test this possibility, we compared overall difference in the proportion of abnormally myelinated axons between TG^+ and their TG^- littermates at P158 by an odds ratio (OR), defining odds as the probability of an abnormally myelinated axon divided by the probability of a normally myelinated one. An OR of 1.0 means that the odds of the outcome occurring is not different than the odds of the outcome not occurring. By estimating the ORs with the logit regression model, we could adjust the logit model to account for the clustering of data within animals, in addition to controlling for confounders and stratifying the analyses when there were significant interactions. Table 1 shows the ORs of abnormally myelinated axons from the logit regression model with an interaction for age and adjustment for clustering of fibers within mice. Adjustment for clustering only affected the standard errors and the values that depended on them, including the *P* value and confidence intervals. The proportion of abnormally myelinated axons was significant in lines 6 (R142W-HA), 153 (R142W), 157 (R142W), and 165 (R142W), but not in line 90 (WT hCx32).

Effects of expressing R142W in a Gjb1-null background

We recently reported that the expression of WT hCx32 largely prevents the development of a demyelinating neuropathy in *Gjb1*-null mice (Scherer et al., 2005). To determine whether R142W or R142W-HA have a comparable effect, we analyzed litters of mice that contain TG^+ and TG^- in *Gjb1*-null background. A blinded observer could not tell the difference between TG^+ and TG^- mice at any age, and the proportion of abnormally myelinated axons in the femoral motor nerve did not appear to be increased around the onset of demyelination (P90) for lines 6, 153, or 157 (Fig. 7B). At P158, however, the time at which demyelination and remyelination are pronounced (Scherer et al., 1998), the odds ratio of finding an abnormally myelinated axon was significantly higher in line 153 (153KO), and not in line 6 (6KO), compared to *Gjb1*-null mice (Table 2 and Fig. 7B). Thus, line 153 may have a dominant effect leading to demyelination that is independent of endogenous/mouse Cx32.

Overexpression of WT hCx32 causes myelin splitting

A different phenotype was observed in lines that express the WT hCx32 protein (90 and 96). In a WT mouse background, many myelin sheaths were split, giving the nerve a “Swiss cheese” appearance in epoxy sections. This finding was much more pronounced in line 96 (Fig. 8A) than in line 90 (Fig. 8B); the former had a higher level of hCx32 than the latter (Fig. 2A). Large myelinated axons throughout the PNS were affected—in the dorsal and ventral roots and in the sciatic and femoral nerves. Electron microscopy demonstrated that the splitting separates compact myelin at the interperiod line, which is contiguous with extracellular space (Figs. 8C and D). In teased fibers and longitudinal sections, splitting appeared to begin and end at incisures, but often extended past intervening incisures (Figs. 8E and F). Macrophages were occasionally seen being the split layers of compact myelin (data not shown). In spite of the large numbers of affected fibers, demyelinated and remyelinated axons were uncommon, indicating that myelin splitting disruption is surprisingly well tolerated.

Discussion

We generated lines of transgenic mice that express the R142W mutant in myelinating Schwann cells. In a *Gjb1*-null background, the mutant protein was exclusively localized to the perinuclear region. In a WT background, the levels of both mutant/human and endogenous/mouse Cx32 protein were decreased, Cx32 was abnormally localized, and the mice developed a progressive demyelinating neuropathy. In contrast, mice expressing WT hCx32 showed increased levels of Cx32 protein, abnormally large aggregates of Cx32 that were normally localized, split myelin sheaths, but few abnormally myelinated axons. These distinct phenotypes demonstrate that the effects of the R142W are intrinsic to the mutation and are not merely the result of overexpression.

The effects of the R142W mutant

This is the first demonstration of a mislocalized Cx32 mutant in myelinating Schwann cells. As in transfected cells (Deschênes et al., 1997), the R142W mutant appears to be retained in the Golgi; it did not appear to reach incisures and paranodes. The

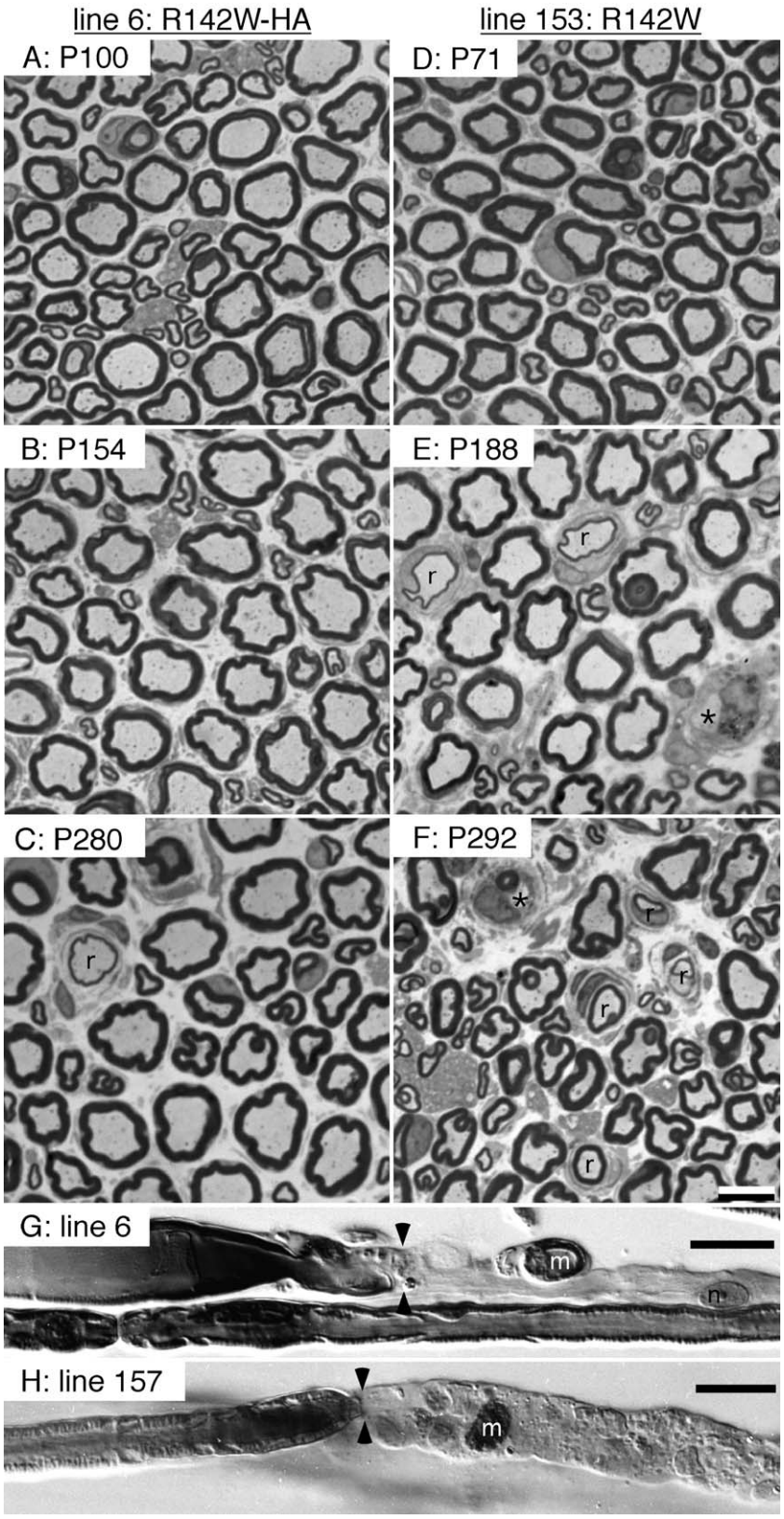

Fig. 6. Expression of R142W causes demyelination of motor axons. These are images of the femoral motor nerve from lines 6 (R142W-HA) and 153 (R142W) at the indicated ages, all in a WT background. The semithin sections show an age-related increase in the number of demyelinated (asterisks) and remyelinated (r) axons, particularly in line 153. The teased fibers show abrupt loss of myelination at nodes of Ranvier (arrows); the demyelinated segments are associated with myelin debris (m) and supernumerary Schwann cells whose nuclei are indicated (n). Scale bar: 10 μm.

Table 1
Quantitative analysis of abnormally myelinated axons in a WT background

TG^- age	%	90 age	%	6 age	%	153 age	%	157 age	%	165 age	%
90	0	90	0	100	0.1	71	0.2	131	0.2	113	0.2
100	0.1	90	0	120	0	71	0.2	131	0.3	113	0.9
131	0	90	0.2	154	0.3	71	0	236	0.6	130	0.8
131	0	90	0	154	0	188	1.2	236	0.2	130	1.0
255	0	266	0	256	0.2	188	1.1	702	0.2	130	1.5
270	0.1	278	0	256	0.3	292	6.1			190	1.0
271	0.1	278	0	255	0.8	416	7.0			271	1.3
275	0	304	0.6	255	0.2	426	10			292	3.4
278	0			280	0.5						
280	0			280	0.7						
292	0			344	1.2						
321	0										
344	0										
TG^+ vs TG^- odds ratio		2.9 $P = 0.275$		15.0 $P < 0.000$		83.1 $P < 0.000$		17.7 $P < 0.000$		71.7 $P < 0.000$	

This table gives the % abnormally myelinated (demyelinated or remyelinated) axons in the femoral motor branch for individual animals, by age (days postnatal). When both the left and the right nerves were available for individual animals (71% of the animals), the numbers were combined. The TG^- (WT) littermates were pooled.

apparent retention of the mutant protein in the Golgi is not unique to R142W: in transfected cells, 20/51 Cx32 mutants are at least partially localized in the Golgi (Yum et al., 2002). Why these Cx32 mutants accumulate in the Golgi is not clear as Cx32 is not known to be modified by Golgi-dependent processes (by glycosylation, for example). Even though Cx32 can oligomerize in the ER (Das Sarma et al., 2002), it is possible that these Cx32 mutants accumulate in the Golgi owing to defective oligomerization. There was no evidence of a generalized abnormality of protein synthesis or trafficking as there were no obvious effects on the distribution and/or levels of other proteins such as Cx29, E-cadherin, claudin-19, MAG, MBP, and P_0. In addition, the ER and Golgi did not contain accumulated material, as reported for myelinating Schwann cells expressing a foreign intrinsic membrane protein (Smit et al., 1996) or a *Pmp22* missense mutation (Dickson et al., 2002).

The decreased level of endogenous/mouse Cx32 was unexpected and leads to the hypothesis that R142W has dominant-negative interactions with endogenous/mouse Cx32. Such an interaction could occur in the ER or the Golgi, both of which have been implicated as sites of oligomerization (Musil and Goodenough, 1993; Kumar et al., 1995; Das Sarma et al., 2002). The presence of one or more mutant subunits in a hemi-channel could result in its mistargeting and/or premature degradation. The similar but milder pathology in TG^+ mice as compared to *Gjb1*-null mice, including the age of onset and the relative sparing of myelinated sensory axons (Anzini et al., 1997; Scherer et al., 1998), supports the postulated dominant-negative interaction. On the other hand, there is no clear relationship between the reduction in Cx32 levels (in immunoblots) and the degree of demyelination (in semithin sections)—Cx32 levels were the lowest in line 6, whereas line 153 had the most abnormally myelinated axons, so the R142W mutant may have additional deleterious effects. The higher numbers of abnormally myelinated axons in 153KO (line 153 in a *Gjb1*-null background) than in *Gjb1*-null mice support the possibility that the R142 mutant has a gain-of-function effect independent of its effects on endogenous Cx32. This effect, however, was not seen in another line (6KO), so it may be the result of a genetic perturbation caused by the site of transgene integration rather than the consequence of the expressed mutant protein. In addition, because the parents of TG^+ mice in a KO background have different genetic backgrounds (the *Gjb1*-null mice were in a C57Bl/6 background, and the transgenic mice were in a FVB/N background), it is possible that background differences contribute to the severity of the neuropathy.

Dominant-negative interactions between R142W and mCx32 (Bruzzone et al., 1994) are non-physiologic as *Gjb1* is subjected to X-inactivation—WT myelinating Schwann cells express only one *Gjb1* allele (Scherer et al., 1998). The relevant dominant-negative interaction may occur between R142W and another connexin that have been proposed to be expressed by myelinating Schwann cells—Cx26, Cx29, and Cx43. Although myelinating Schwann cells have been reported to express Cx26 and Cx43 (Yoshimura et al., 1996; Zhao and Spray, 1998; Mambetisaeva et al., 1999), these results are controversial (Satake et al., 1997) and remain to be definitely demonstrated. The human ortholog of mCx29, hCx31.3, is a strong candidate as mCx29 is well documented to be expressed by myelinating Schwann cells (Söhl et al., 2001; Altevogt et al., 2002; Li et al., 2002). Cx29, however, does not appear to form functional gap junctions by itself (Altevogt et al., 2002), and as we show here, its localization was not affected by the R142W mutant in myelinating Schwann cells. To date, there is no genetic evidence for a role of another connexin besides Cx32 in myelinating Schwann cells.

A dominant interaction between R142W and hCx47, however, may be the basis for a rare clinical problem in CMT1X patients. R142W is one of the few *GJB1* mutations associated with transient neurological deficits that are accompanied by abnormally magnetic resonance imaging of the CNS white matter (Paulson et al., 2002; Taylor et al., 2003). The Cx32 mutants associated with this phenotype (T55I, R75W, E102del, R142W, R164Q, C168Y) are retained in the ER or Golgi (Kleopa et al., 2002; Yum et al., 2002; Scherer, unpublished). If abnormal interactions between these Cx32 mutants and WT hCx47, another connexin expressed by oligodendrocytes (Menichella et al., 2003; Odermatt et al., 2003), diminish the function of Cx47, then this could cause CNS dysfunction. Recessive *GJA12/Cx47* mutations cause a severe dysmyelinating disease known as Pelizaeus–Merzbacher-like disease (Uhlenberg et al., 2004); the corresponding Cx47 mutants

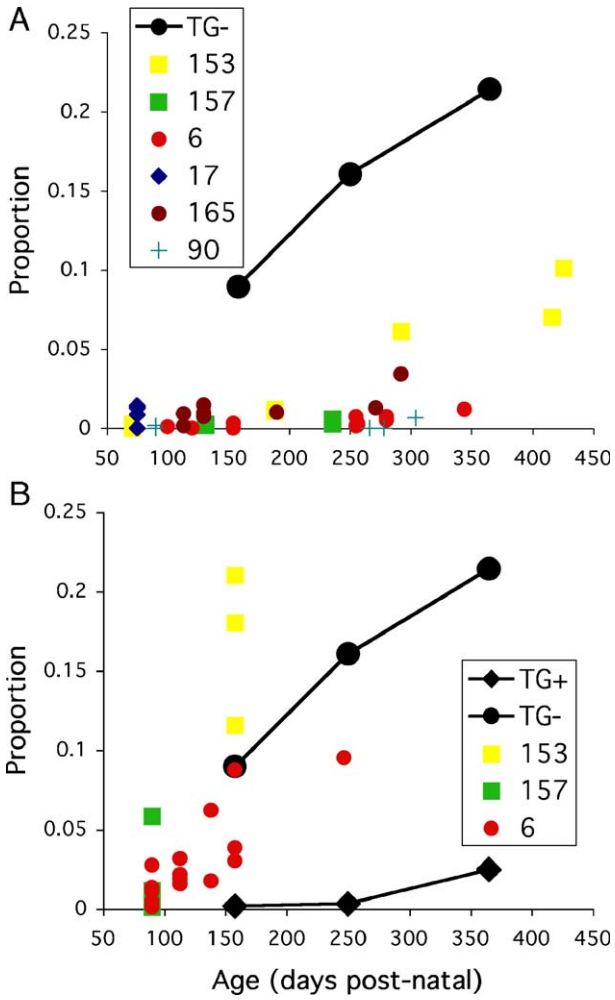

Fig. 7. The proportion of abnormally myelinated axons in femoral motor nerves. These plots show the proportion of abnormally myelinated axons in the femoral motor nerves in mice at different ages. Panel A shows the effects of different transgenes in a WT background; each point represents a single animal (these data are listed in Table 1). Panel B shows the effects of different transgenes in a *Gjb1*-null background; each point represents a single animal (these data are listed in Table 2). For comparison, the data for *Gjb1*-null mice that express WT hCx32 (line 90; TG^+) and their *Gjb1/cx32*-null littermates (TG^-) are shown as means connected by lines (Scherer et al., 2005).

do not form functional gap junctions (Orthmann and Scherer, unpublished observations).

Overexpression of WT hCx32 causes myelin splitting

Split myelin sheaths appear to be a consequence of Cx32 overexpression in incisures: splitting typically begins and ends at incisures, where Cx32 accumulates in TG^+ mice. Splitting is not specific to Cx32 overexpression as it has been found in diverse pathological settings—in toxic neuropathies (Myers et al., 1982; Feldman et al., 1992; Mizisin and Powell, 1993; Tonkin et al., 2000), in diabetes (Mizisin et al., 1998), and in other kinds of mutant mice (Coetzee et al., 1996; Gravel et al., 1996; Yin et al., 1997). In each example, separation occurs at the intraperiod line, which is formed by the apposed cell membranes that are held together by *cis* and *trans* interactions between P_0 tetramers (Shapiro et al., 1996). The cause of splitting in our transgenic mice, and in these other examples, remains to be elucidated. One possibility is that the large amount of Cx32 destabilizes the adhesion between the layers of the myelin sheath, although the localization of one protein that may play a role in this regard, E-cadherin, did not appear to be affected (Supplemental Fig. 2).

The cellular and molecular basis of connexin mutations

Dominant and/or recessive mutations of nine of the twenty human connexin genes cause hereditary diseases in humans. In each case, the phenotype appears to be cell-autonomous—affected cells express the mutant connexin. In addition to demyelinating diseases discussed above, various skin diseases are caused by mutations in the genes encoding *GJB2/Cx26*, *GJB6/Cx30*, *GJB4/Cx30.3*, and *GJB3/Cx31*, all of which are expressed in skin (Kelsell et al., 2001). Similarly, mutations in *GJB2/Cx26*, *GJB6/Cx30*, and *GJB3/Cx31* cause hearing loss (http://webhost.ua.ac.be/hhh/); these connexins are expressed in the cochlea (Buniello et al., 2004). Dominant mutations in *GJA3/Cx46* and *GJA8/Cx50* cause cataracts, both of which are expressed in the lens (White, 2002). Finally, mutations in *GJA1/Cx43* cause oculodentodigital dysplasia, a syndrome affecting different tissues, all of which express Cx43 (Paznekas et al., 2003; Richardson et al., 2004).

The high degree of homology between connexins provides an opportunity to compare mutations affecting homologous residues. Comparing *GJB1* and *GJB2/Cx26* mutations is illuminating as these two are highly homologous and are both affected by many

Table 2
Quantitative analysis of abnormally myelinated axons in a KO background

TG^-		90KO		6KO		153KO	
Age	%	Age	%	Age	%	Age	%
158	12	158	0	90	0.1	158	12
158	8.9	158	0.2	90	1.1	158	18
158	5.6	158	0.3	90	0.3	158	21
250	16	250	0.2	90	2.7		
250	16	250	0.4	90	0.4		
365	16	365	2.2	90	0.5		
365	27	365	4.4	90	1.3		
		365	3.0	113	2.2		
				113	3.2		
				113	1.5		
				113	1.9		
				138	1.8		
				138	6.2		
				158	3.0		
				158	8.7		
				158	3.8		
				247	9.5		
TG^- vs TG^+ KO at P158 odds ratio		0.01 $P < 0.000$		0.51 $P = 0.069$		2.01 $P = 0.003$	

This table gives the % abnormally myelinated axons (demyelinated or remyelinated) in the femoral motor branch for individual animals, by age (days post-natal), for lines 90 (WT hCx32; data from Scherer et al., 2005), 6 (R142W-HA) and 153 (R142W), all in a KO background. When both the left and the right nerves were available for individual animals (83% of the animals), the numbers were combined. Compared to TG^- mice at P158 (Scherer et al., 2005), TG^+ 90KO mice have significantly fewer, and TG^+ 153KO have significantly more, abnormally myelinated axons, respectively.

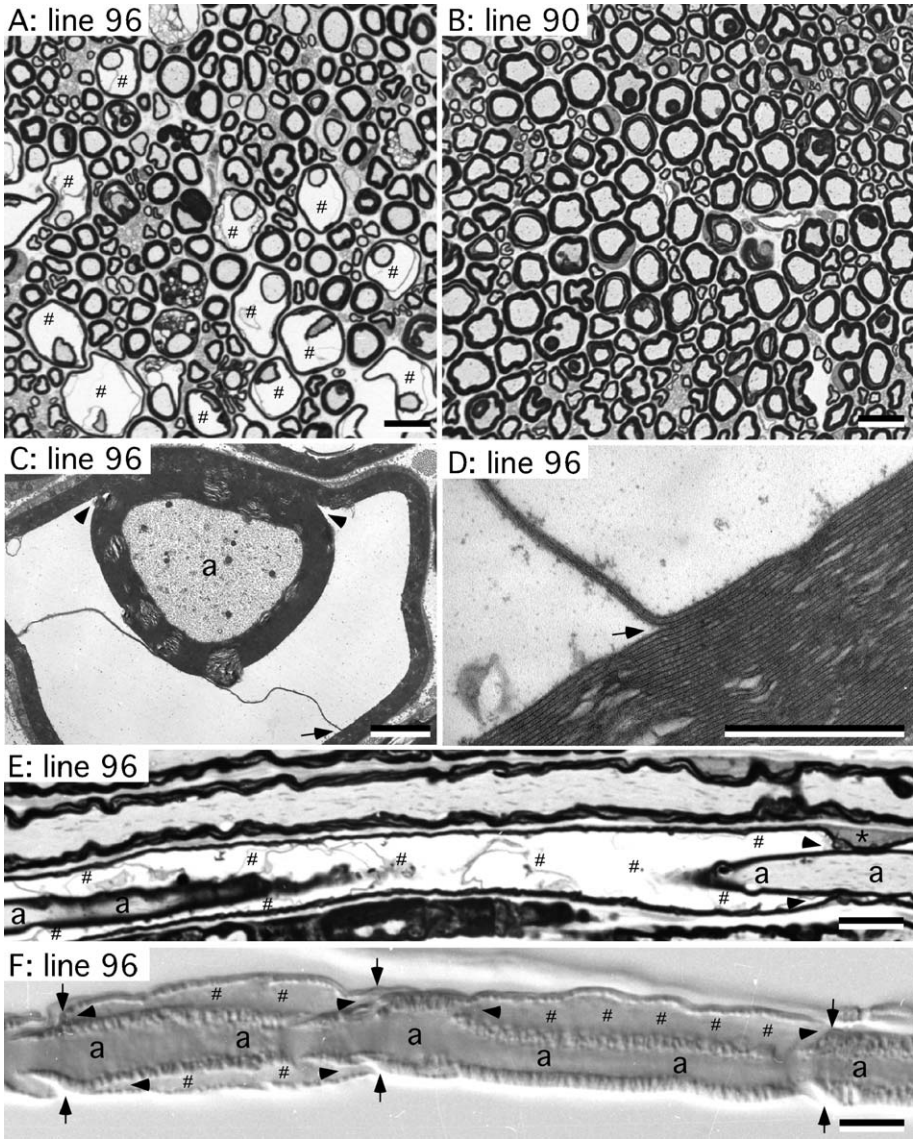

Fig. 8. Transgenic mice overexpressing WT hCx32 in a WT background develop split myelin sheaths. These are photomicrographs (A, B, E, semithin sections of sciatic nerve; F, teased ventral root fibers) and electron micrographs (C and D; thin sections of sciatic nerve) from 9-month-old mice from two different transgenic lines. Line 96 has many split myelin sheaths (# mark the spaces between the splits); these are not present in line 90. In transverse sections (A and C), the split myelin sheaths are usually attached circumferentially in one region (between arrowheads in panel C), and electron microscopy demonstrates that the separation occurs in the interperiod line (arrows in panels C and D). In longitudinal sections and teased fibers, the site of myelin sheath splitting (arrowheads) appears to originate at incisures (marked by apposed arrows in panel F). In panels C–F, the axon (a) and Schwann cell nucleus (asterisk) are indicated. Scale bars: A and B: 10 μm; C: 2 μm; D: 0.5 μm; E and F: 10 μm.

mutations. Because no polymorphisms (at the amino acid level) in *GJB1* have been identified and most Cx32 mutants analyzed to date have altered functional characteristics (Abrams et al., 2000), many of the putative polymorphisms of *GJB2/Cx26* (http://webhost.ua.ac.be/hhh/) are likely to alter the function of Cx26 and hence be recessive alleles. Four of six amino acids in Cx32 in which amino acid substitutions cause a transient CNS phenotype are also affected by missense mutations in Cx26 that cause hearing loss and/or skin disease (Cx32/Cx26: R75/R75, R142/R143, R164/R165, and C168/C169), and three of these are dominant (R75W, R75Q, R143Q). Mutations in certain conserved residues, such as R75 (in Cx32), also cause dominant phenotypes in *GJA1/Cx43* (Paznekas et al., 2003). However, there are other examples of mutations affecting a conserved amino acid having different effects (dominant in one connexin and recessive in another) and mutations of residues that are less conserved causing dominantly or recessive phenotypes. It will be interesting to compare the cellular effects of similar mutations of different connexin genes as more data become available.

Conclusion

The mutant R142W TG^{+} mice are a model of dominant effects of CMT1X mutations and complement *Gjb1*-null mice, which are a model of loss of function effects. Distinguishing dominant effects from loss of function is key to the development of rational treatments for the manifestations of CMT1X. Gene replacement

approaches may benefit individuals with loss of function mutations in *GJB1*, but not those who have mutations with dominant effects.

Experimental methods

Generation of TG$^+$ mutant mice

The creation of mice expressing a *GJB1* mutation (R175 frameshift) with a 1.1 kb rat *Mpz/P0* promoter fused to the human *GJB1* gene has been described (Abel et al., 1999; Scherer et al., 2005). We used a similar strategy to generate the R142W mutation. A genomic clone of *GJB1* was isolated from a human X chromosome genomic library, a fragment containing exon 1b, exon 2, and a 356 bp intron was isolated, removing the TATAA box of the P2 promoter (Fig. 1A). A 1.1 kb fragment containing the rat *Mpz* promoter (Lemke et al., 1988), which drives expression in myelinating Schwann cells in TG$^+$ mice (Messing et al., 1992), was purified and ligated upstream of the *Nde*I/*Sac*I Cx32 fragment in the appropriate orientation; this clone was designated P0Cx32WT (Fig. 1B). Further cloning steps were performed to introduce the R142W mutation and a nine amino acid hemagglutinin (HA) epitope tag (Wilson et al., 1984) at the carboxy-terminus of the mutant protein (Higuchi, 1990; Kolodziej and Young, 1991). A fragment containing the R142W mutation was isolated from a family 243 clone (Bergoffen et al., 1993; Bruzzone et al., 1994) and was used to replace the equivalent fragment in the P0Cx32WT clone, resulting in a clone designated P0243. Next, PCR site-directed mutagenesis was used to replace the stop codon with an *Asc*I site. The resulting clone was then cut with *Asc*I, and a 47 bp oligonucleotide encoding an in-frame HA epitope tag was inserted followed by stop codons in all three reading frames. This clone was designated P0243HA. The cloning sites, orientation, and in-frame positioning of the epitope tag were confirmed by sequencing.

A 6.4 kb transgene cassette for each clone was released from vector sequences by digestion with *Apa*I and *Nsi*I. The fragment was isolated, purified, and microinjected into the male pronucleus of fertilized eggs obtained from FVB/N mice (Taketo et al., 1991; Taconic Farms, Germantown, NY), according to standard protocols (Brinster et al., 1985). Eggs that survived microinjection were then placed into pseudopregnant foster mice for gestation. To genotype mice, DNA (10 μg) was isolated from tail clips, digested with *Taq*I, electrophoresed in a 1% agarose gel, transferred to a nylon membrane (Zetabind transfer membrane, CUNO, Meriden, CT), and hybridized with a 613 bp *Bgl*II/*Cla*I probe from the *Mpz/P0* promoter. Southern blot analysis was used to genotype the founders: DNA (10 μg) from tail biopsies was digested with *Taq*I, electrophoresed in a 1% agarose gel, transferred to a nylon membrane (Zetabind transfer membrane, CUNO, Meriden, CT), and hybridized with a 613 bp *Bgl*II/*Cla*I probe from the *Mpz* promoter. TG$^+$ founders had a 648 bp junction fragment, whereas the endogenous *Mpz* produced a 3.2 kb fragment. TG$^+$ progeny were identified by PCR with transgene-specific primers (Fig. 1)—<P0> (5′-CAG TTC CTT GTC CCC CGC TCT CTC-3′), which recognizes the 24 bp immediately 3′ of the transcription start point, and <2> (5′-TTG CTG GTG AGC CAC GTG CAT GGC-3′), a sequence within the open reading frame of *Cx32*, using the following conditions: 94°C × 5 min, 35 cycles of 94°C × 1 min, 66°C × 1 min, 72°C × 1 min, then 72°C × 10 min. An 872 bp product confirmed the presence of the transgene.

The generation and characterization of *Gjb1*-null (*Gjb1*$^{-/-}$ female and *Gjb1*$^{-/Y}$ male) mice have been described (Nelles et al., 1996; Anzini et al., 1997; Scherer et al., 1998). Breeding pairs of animals were obtained from Dr. Klaus Willecke then propagated at the University of Pennsylvania. Genotypes were done by PCR analysis of genomic DNA isolated from tail clips (Anzini et al., 1997) and confirmed by Southern blot analysis. Heterozygous mutant TG$^+$ males from selected transgenic lines were crossed with *Gjb1*$^{-/-}$ females (Nelles et al., 1996). About 50% of the resulting *Gjb1*$^{-/Y}$ male offspring were TG$^+$, in accordance with Mendelian genetics. The *Gjb1*-null mice were bred in a C57Bl/6 background, whereas the transgenic mice were made in a FVB/N background, so that the offspring of this cross were a mixture of these backgrounds. The severity of the neuropathy in *Gjb1*-null mice has not been investigated in different genetic backgrounds in mice.

Reverse transcription-polymerase chain reaction (RT-PCR)

Total RNA was isolated from snap-frozen sciatic nerves according to the RNAzol™ B (Tel-Test, Inc., Friendswood, TX) protocol for small amounts of tissue and quantitated by spectrophotometry. Reverse transcription was performed using 0.5–1 μg of RNA, random primer p(dN)$_6$ (Boehringer Mannheim, Indianapolis, IN), avian myeloblastosis virus (AMV) reverse transcriptase (Promega, Madison, WI), AMV RT (5×) reaction buffer (Promega), RNAse inhibitor (Boehringer Mannheim, Indianapolis, IN), and deoxynucleotide triphosphates (dNTPs; Ultrapure dNTP set, Pharmacia Biotech, Piscataway, NJ). Subsequent amplification of cDNA with primers (Fig. 1B) <1> (5′-TGA GGC AGG ATG AAC TGG ACA GGT-3′) and <4> (5′-CAC GAA GCA GTC CAC TGT-3′) resulted in a 553 bp PCR product. The following PCR conditions were used for primers <1> and <4>: 94°C × 5 min, 40 cycles of 94°C × 1 min, 60°C × 1 min, 72°C × 1 min, then 72°C × 10 min. *Msc*I cuts the human PCR product into two fragments (280 and 273 bp); *Hha*I cuts the mouse PCR product into two fragments (230 and 323 bp). Digestion of RT-PCR product with *Msc*I or *Hha*I allowed determination of the relative mRNA expression level of the transgene to the endogenous gene by densitometry of the mouse- and human-specific bands within a single lane.

Immunoblot analysis

Protein was isolated from snap-frozen sciatic nerves (from juveniles to adults, 1–6 months old), crushed in a mortar and pestle on dry ice, suspended in Tris-buffered sodium dodecyl sulfate (SDS) lysis buffer (50 mM Tris, pH 7.0/1% SDS/0.017 mg/ml phenylmethyl sulfonyl fluoride) with or without 6 M urea, and sonicated (Sonic Dismembranator, Fisher Scientific, Pittsburgh, PA). Protein was also isolated from Cos cells (Deschênes et al., 1997) that had been transiently transfected to express WT hCx32 with or without an HA-tag. Samples were spun at 4°C to pellet insolubles, and the supernatant was quantitated by DC protein assay (BioRad, Hercules, CA). 100 or 200 μg of protein per lane was loaded onto 12% SDS-PAGE gels, run at 10–20 mA overnight at room temperature with size markers (Rainbow markers, Amersham Life Sciences, Buckinghamshire, England). Semi-dry transfer (FisherBiotech, Pittsburgh, PA) to a nylon membrane (Immobilon-P transfer membrane, Millipore, Bedford, MA) was completed following the recommendations of Millipore and analyzed by immunoblot analysis (Scherer et al., 1995). Primary antibodies were either diluted in 5% milk in Tris-buffered saline (TBS) or used as straight hybridoma supernatant. Primary antibodies included the mouse monoclonal antibody 7C6.C7 against Cx32 (undiluted hybridoma supernatant; Li et al., 1997), rabbit antiserum against Cx32 (diluted 1:1000; Zymed, South San Francisco, CA), the HA tag (Y-11, diluted 1:500; Santa Cruz Biotechnology, Inc., Santa Cruz, CA), myelin basic protein (MBP, diluted 1:2000; DeFerra et al., 1985), and P$_0$ (diluted 1:500,000; D'Urso et al., 1990). Secondary antibodies were peroxidase-coupled goat anti-mouse IgG1 heavy chain (1:2500 dilution; Southern Biotechnology Associates, Inc., Birmingham, AL) or goat F(ab′)$_2$ anti-rabbit IgG (1:2500 dilution; Jackson ImmunoResearch Laboratories, Inc., West Grove, PA). Membranes were developed by enhanced chemiluminescence methods (Amersham Life Sciences, Piscataway, NJ) and exposed to autoradiography film (Kodak Scientific Imaging film, Rochester, NY, X-OMAT AR). The relative levels of protein expression were measured by densitometry (Molecular Dynamics computing densitometer model 300A) and interactive computer software (Image Quant, Molecular Dynamics). Values were corrected for loading variation by quantitation of the P$_0$ band on the Coomassie-stained gel.

Immunohistochemistry

Sciatic nerves from adult mice were removed and placed into either 4% paraformaldehyde in phosphate-buffered saline (PBS) for 5–30 min or phosphate-buffered saline at 4°C, teased to small groups of fibers on glass

slides (Fisherbrand Superfrost/Plus microscope slides, Fisher Scientific, Pittsburgh, PA), and air-dried at room temperature overnight. Fibers were permeabilized in −20°C acetone for 10 min, washed in TBS three times, blocked in 5% fish skin gelatin (Sigma, St. Louis, MO) containing 0.1% Triton-X and 0.04% sodium azide in PBS for at least 1 h at room temperature, and incubated in the appropriate primary antibody diluted in 5% fish skin gelatin at 4°C for 16–48 h. We used mouse monoclonal antibodies against Cx32 [7C6.C7, diluted at 1:1 (Scherer et al., 2005) or M12.13, diluted 1:1 (Goodenough et al., 1988)], hemagglutin (12CA5, diluted 1:10), 58 kDa Golgi protein (Sigma, St. Louis, MO, diluted 1:50), and MAG (clone 513, Boehringer Mannheim, Indianapolis, IN, diluted 1:100), as well as rat monoclonal antibodies against E-cadherin (DECMA, Sigma, St. Louis, MO, diluted 1:50) and hemagglutin (Roche, Indianapolis, IN, diluted 1:50), and rabbit antisera against hemagglutin (Y-11, diluted 1:100; Santa Cruz Biotechnology, Inc., Santa Cruz, CA), Cx29 (Altevogt et al., 2002), Cx32 ("Lola"; gift of David Paul, diluted 1:200; Zymed, South San Francisco, CA, diluted 1:200, Chemicon, Temecula, CA, diluted 1:200), E-cadherin (diluted 1:500; (Fannon et al., 1995), MAG (diluted 1:500; (Pedraza et al., 1990), claudin-19 (diluted 1:600; (Miyamoto et al., 2005), MBP (diluted 1:500; (DeFerra et al., 1985), P_0 (diluted 1:1000; (D'Urso et al., 1990), and medial Golgi 160 protein (diluted 1:500; (Gonatas et al., 1989). Following incubation in the primary antibody, the samples were washed three times for 5 min in TBS, incubated for 1–2 h in the appropriate secondary antibody (either rhodamine-conjugated donkey anti-mouse or fluorescein-conjugated donkey anti-rabbit antibodies (diluted 1:100; Jackson ImmunoResearch Laboratories, West Grove, PA), washed in TBS, counterstained for 2 min in DAPI (4,6-diamidino-2-phenylindole; Sigma), and rinsed in water before mounting in Vectashield Mounting Medium (Vector Laboratories, Inc., Burlingame, CA) and coverslipped. These preparations were imaged with epifluorescence TRITC and FITC optics on a Leica DMR light microscope equipped with a cooled Hamamatsu camera (Bridgewater, NJ) using Metamorph Imaging System (West Chester, PA) or OpenLab (Improvision, Lexington, MA) software or with a Leica TCS laser scanning confocal microscope followed by image manipulation with Adobe Photoshop (San Jose, CA).

Quantitative analysis

Adult animals were euthanized with an i.p. injection of pentobarbital and perfused with 0.9% NaCl followed by 3% glutaraldehyde in 0.1 M phosphate buffer (pH 7.4). Femoral and sciatic nerves, the cauda equina, and single dorsal and ventral roots were removed and placed in fresh fixative overnight at 4°C. The samples were washed twice in 0.1 M phosphate buffer (pH 7.4) then placed in 2% osmium tetroxide in 0.1 M phosphate buffer for 1 h. Nerves and cauda equinas were rinsed in water, dehydrated with successively increasing percentages of ethanol, followed by propylene oxide, infiltrated in 50% and 75% epoxy in propylene oxide, then 100% epoxy overnight, embedded in fresh epoxy, and hardened in a 60°C oven. Semithin sections (500 nm) were stained with 1% toluidine blue and photographed on a Leica DMR microscope. Thin sections (80 nm) were stained with lead citrate and uranyl acetate and photographed on a Zeiss EM10 electron microscope. Nerve roots were washed in 0.1 M PB, placed into successively increasing percentages of glycerol overnight (33, 66, and 100%) at 45°C, and teased with fine needles and a dissecting microscope, mounted in glycerin, and photographed using differential interference optics on a Leica DMR microscope. Images were scanned and manipulated in Adobe Photoshop.

We counted the number of demyelinated, remyelinated, and normally myelinated axons from semithin sections of the femoral motor branch. Axons larger than 1 μm in diameter without a myelin sheath were considered demyelinated. Axons with myelin sheaths that were less than 10% of the axonal diameter as well as myelinated axons that were surrounded by "onion bulbs" (circumferentially arranged Schwann cell processes and extracellular matrix) were considered remyelinated. The rest of the myelinated axons were considered to be normally myelinated. Either a digital image or a photographic montage of each nerve was prepared, and the total number of myelinated axons was counted from the photograph, re-examining the section as necessary to classify ambiguous axons. Repeated counts of one affected nerve were essentially identical (within 1%). We also performed counts in two affected nerves at intervals of more than 1 mm apart; the proportion of abnormal axons in a single nerve varied little—5.6%, 6.6%, and 5.2% for one nerve and 3.2% and 2.5% for another. The proportion of abnormally myelinated (demyelinated and remyelinated) axons in TG^+ versus their non-transgenic (TG^-) littermates was compared statistically, both in a WT (Table 1) and a *Gjb1/cx32*-null (Table 2) background.

Injection of 5,6-carboxyfluorescein

We analyzed the intracellular movement of 5,6-carboxyfluorescein (5,6-CF, Sigma, St. Louis, MO), a fluorescent dye of small molecular mass (376 Da) as previously described (Balice-Gordon et al., 1998). 5,6-CF was initially dissolved in 3 M KOH at a concentration of 50 mg/ml then diluted to 5 mg/ml in a 1.5 M buffered KCl solution. Young adult mice (5–7 weeks old) were sacrificed; both sciatic nerves were removed and placed in oxygenated, ice-cold Liley's mammalian Ringer solution (136.8 mM NaCl, 5 mM KCl, 2 mM $CaCl_2$, 1 mM $MgCl_2$, 24 mM $NaHCO_3$, 1 mM NaH_2PO_4, and 11 mM glucose; Hubbard et al., 1969). Nerve segments, approximately 1 cm long, were teased into small bundles on polystyrene disks that were etched to have a 10 × 10 grid, each approximately 1 mm^2. The disk was mounted on the stage of a modified Leica fluorescence microscope (Balice-Gordon et al., 1998) and bubbled with 95% O_2/5% CO_2 mixture at room temperature. Nuclei of myelinating axons were visualized by adding Hoechst (bis-benzamide) vital dye (Molecular Probes, Inc., Eugene, OR) to the bath. 5,6-Carboxyfluorescein (5,6-CF, Sigma, St. Louis, MO, molecular mass 376 Da) was injected into the perinuclear cytoplasmic region through a glass micropipette (Sutter Instrument Co., USA). The resting membrane potential of the cells was recorded on entry and/or exit, and those Schwann cells with a resting potential of less than −4 mV were excluded from this study. At least 5 Schwann cells meeting this criterion were obtained for the *Gjb1/cx32* knockout animals and for each transgenic line. Dye was injected by iontophoresis, and images were taken using a low light level SIT camera (Dage-MTI), a PC-based image processing system, and Metamorph Imaging System interactive software (West Chester, PA). For all experiments, we successfully injected dye into 72% of the attempted Schwann cells. Entire planes of figures were enhanced, filtered, and cropped with Adobe Photoshop.

Acknowledgments

This work was supported by the Medical Scientist Training Program (to L.J.B.), RO1 NS08075 (to K.F. and S.S.S.), and RO1 NS42878 (to S.S.S.). We are grateful to Marion Oronzi Scott and Drs. Suzanne Deschênes and Diane Merry for helpful discussions, Qian Chen, Melissa Davey, Jennifer Orthmann, Sharon Seltzer, Erich Sirkowski, Denise Springman, Suping Wang, and Ted Xu for technical assistance, Dr. Larry Wrabetz for the gift of the *Mpz* promoter and advice on PCR site-directed mutagenesis, Dr. Klaus Willecke for the gift of the *Gjb1/cx32* knockout mice, and Drs. David Colman, Nicholas Gonatas, Elliot Hertzberg, Thomas Kadesch, John Kamholz, Tatsuo Miyamo, David Paul, James Salzer, and Shoichiro Tsukita for their generous gifts of antibodies.

Appendix A. Supplementary data

Supplementary data associated with this article can be found, in the online version, at doi:10.1016/j.mcn.2006.05.001.

References

Abel, A., Bone, L.J., Messing, A., Scherer, S.S., Fischbeck, K.H., 1999. Studies in transgenic mice indicate a loss of connexin32 function in X-linked Charcot–Marie–Tooth disease. J. Neuropathol. Exp. Neurol. 58, 702–710.

Abrams, C.K., Oh, S., Ri, Y., Bargiello, T.A., 2000. Mutations in connexin 32: the molecular and biophysical bases for the X-linked form of Charcot–Marie–Tooth disease. Brain Res. Rev. 32, 203–214.

Abrams, C.K., Freidin, M.M., Verselis, V.K., Bennett, M.V.L., Bargiello, T.A., 2001. Functional alterations in gap junction channels formed by mutant forms of connexin 32: evidence for loss of function as a pathogenic mechanism in the X-linked form of Charcot–Marie–Tooth disease. Brain Res. 900, 9–25.

Ainsworth, P.J., Bolton, C.F., Murphy, B.C., Stuart, J.A., Hahn, A.F., 1998. Genotype/phenotype correlation in affected individuals of a family with a deletion of the entire coding sequence of the connexin 32 gene. Hum. Genet. 103, 242–244.

Altevogt, B.M., Kleopa, K.A., Postma, F.R., Scherer, S.S., Paul, D.L., 2002. Cx29 is uniquely distributed within myelinating glial cells of the central and peripheral nervous systems. J. Neurosci. 22, 6458–6470.

Anzini, P., Neuberg, D.H.-H., Schachner, M., Nelles, E., Willecke, K., Zielasek, J., Toyka, K., Suter, U., Martini, R., 1997. Structural abnormalities and deficient maintenance of peripheral nerve myelin in mice lacking the gap junction protein connexin32. J. Neurosci. 17, 4545–4561.

Arroyo, E.J., Xu, Y.-T., Zhou, L., Messing, A., Peles, E., Chiu, S.Y., Scherer, S.S., 1999. Myelinating Schwann cells determine the internodal localization of Kv1.1, Kv1.2, Kvβ2, and Caspr. J. Neurocytol. 28, 333–347.

Balice-Gordon, R.J., Bone, L.J., Scherer, S.S., 1998. Functional gap junctions in the Schwann cell myelin sheath. J. Cell Biol. 142, 1095–1104.

Bergoffen, J., Scherer, S.S., Wang, S., Oronzi-Scott, M., Bone, L., Paul, D.L., Chen, K., Lensch, M.W., Chance, P., Fischbeck, K., 1993. Connexin mutations in X-linked Charcot–Marie–Tooth disease. Science 262, 2039–2042.

Brinster, R.L., Chen, H.Y., Trumbauer, M.E., Yagle, M.K., Palmiter, R.D., 1985. Factors affecting the efficiency of introducing foreign genes into mice by microinjecting eggs. Proc. Natl. Acad. Sci. U. S. A. 82, 4438–4442.

Brinster, R.L., Allen, J.M., Behringer, R.R., Gelinas, R.E., Palmiter, R.D., 1988. Introns increase transcriptional efficiency in transgenic mice. Proc. Natl. Acad. Sci. U. S. A. 85, 836–840.

Bruzzone, R., White, T.W., Scherer, S.S., Fischbeck, K.H., Paul, D.L., 1994. Null mutations of connexin32 in patients with X-linked Charcot–Marie–Tooth disease. Neuron 13, 1253–1260.

Bruzzone, R., White, T.W., Paul, D.L., 1996. Connections with connexins: the molecular basis of direct intercellular signaling. Eur. J. Biochem. 238, 1–27.

Buniello, A., Montanaro, D., Volinia, S., Gasparini, P., Marigo, V., 2004. An expression atlas of connexin genes in the mouse. Genomics 83, 812–820.

Coetzee, T., Fujita, N., Dupree, J., Shi, R., Blight, A., Suzuki, K., Suzuki, K., Popko, B., 1996. Myelination in the absence of galactocerebroside and sulfatide: normal structure with abnormal function and regional instability. Cell 86, 209–219.

Das Sarma, J., Wang, F.S., Koval, M., 2002. Targeted gap junction protein constructs reveal connexin-specific differences in oligomerization. J. Biol. Chem. 277, 20911–20918.

DeFerra, F., Engh, H., Hudson, L., Kamholz, J., Puckett, C., Molineaux, S., Lazzarini, R.A., 1985. Alternative splicing accounts for the four forms of myelin basic protein. Cell 43, 721–727.

Deschênes, S.M., Walcott, J.L., Wexler, T.L., Scherer, S.S., Fischbeck, K.H., 1997. Altered trafficking of mutant connexin32. J. Neurosci. 17, 9077–9084.

Dickson, K.M., Bergeron, J.J.M., Shames, I., Colby, J., Nguyen, D.T., Chevet, E., Thomas, D.Y., Snipes, G.J., 2002. Association of calnexin with mutant peripheral myelin protein-22 ex vivo: a basis for "gain-of-function" ER diseases. Proc. Natl. Acad. Sci. U. S. A. 99, 9852–9857.

D'Urso, D., Brophy, P.J., Staugaitis, S.M., Gillespie, C.S., Frey, A.B., Stempak, J.G., Colman, D.R., 1990. Protein zero of peripheral nerve myelin: biosynthesis, membrane insertion, and evidence for homotypic interaction. Neuron 4, 449–460.

Dyck, P.J., Dyck, P.J.B., Engelstad, J., 2005. Pathologic alterations of nerves. In: Dyck, P.J., Thomas, P.K., Eds. Peripheral Neuropathy, vol. 1, 2nd ed. Elsevier Saunders, Philadelphia, pp. 733–829.

Fannon, A.M., Sherman, D.L., Ilyina-Gragerova, G., Brophy, P.J., Friedrich, V.L., Colman, D.R., 1995. Novel E-cadherin mediated adhesion in peripheral nerve: Schwann cell architecture is stabilized by autotypic adherens junctions. J. Cell Biol. 129, 189–202.

Feldman, D., Brosnan, C., Anderson, T.D., 1992. Ultrastructure of peripheral neuropathy induced in rabbits by 2′,3′-dideoxycytidine. Lab. Invest. 66, 75–85.

Gonatas, J.O., Mezitis, S.G.E., Stieber, A., Fleischer, B., Gonatas, N.K., 1989. MG-160: a novel sialoglycoprotein of the medial cisternae of the Golgi apparatus. J. Biol. Chem. 164, 646–653.

Goodenough, D.A., Paul, D.L., Jesaitis, L., 1988. Topological distribution of two connexin32 antigenic sites in intact and split rodent hepatocyte gap junctions. J. Cell Biol. 107, 1817–1824.

Gravel, M., Peterson, J., Yong, V.W., Kottis, V., Trapp, B., Braun, P.E., 1996. Overexpression of 2′,3′-cyclic nucleotide 3′-phosphodiesterase in transgenic mice alters oligodendrocyte development and produces aberrant myelination. Mol. Cell. Neurosci. 7, 453–466.

Higuchi, R., 1990. Recombinant PCR. In: Innis, M.A., Gelfand, D.H., Sninsky, J.J., White, T.J. (Eds.), PCR Protocols: A Guide to Methods and Applications. Academic Press, Inc., San Diego, pp. 177–183.

Huang, Y., Sirkowski, E.E., Stickney, J.T., Scherer, S.S., 2005. Prenylation-defective human connexin32 mutants are normally localized and function equivalently to wild type connexin32 in myelinating Schwann cells. J. Neurosci. 25, 7111–7120.

Hubbard, J.I., Llinas, R., Quastel, D.M.J., 1969. Monographs of the Physiological Society: Electrophysiological Analysis of Synaptic Transmission. Edward Arnold, London, pp. 299–310.

Kelsell, D.P., Di, W.L., Houseman, M.J., 2001. Connexin mutations in skin disease and hearing loss. Am. J. Hum. Genet. 68, 559–568.

Kleopa, K.A., Yum, S.W., Scherer, S.S., 2002. Cellular mechanisms of connexin32 mutations associated with CNS manifestations. J. Neurosci. Res. 68, 522–534.

Kolodziej, P.A., Young, R.A., 1991. Epitope tagging and protein surveillance. In: Guthrie, C., Fink, G. (Eds.), Methods in Enzymology: Guide to Yeast Genetics and Molecular Biology, vol. 194. Academic Press, Inc., San Diego, pp. 508–519.

Kumar, N.M., Friend, D.S., Gilula, N.B., 1995. Synthesis and assembly of human β1 gap junctions in BHK cells by DNA transfection with the human β1 cDNA. J. Cell Sci. 108, 3725–3734.

Lemke, G., Lamar, E., Patterson, J., 1988. Isolation and analysis of the gene encoding for peripheral myelin protein zero. Neuron 1, 73–83.

Leone, D.P., Genoud, S., Atanasoski, S., Grausenburger, R., Berger, P., Metzger, D., Macklin, W.B., Chambon, P., Suter, U., 2003. Tamoxifen-inducible glia-specific Cre mice for somatic mutagenesis in oligodendrocytes and Schwann cells. Mol. Cell. Neurosci. 22, 430–440.

Li, J., Hertzberg, E.L., Nagy, J.I., 1997. Connexin32 in oligodendrocytes and association with myelinated fibers in mouse and rat brain. J. Comp. Neurol. 379, 571–591.

Li, X., Lynn, B.D., Olson, C., Meier, C., Davidson, K.G.V., Yasumura, T., Rash, J.E., Nagy, J.L., 2002. Connexin29 expression, immunocytochemistry and freeze-fracture replica immunogold labelling (FRIL) in sciatic nerve. Eur. J. Neurosci. 16, 795–806.

Liang, G.S.L., de Miguel, M., Gomez-Hernandez, J.M., Glass, J.D., Scherer, S.S., Mintz, M., Barrio, L.C., Fischbeck, K.H., 2005. Severe neuropathy with leaky connexin32 hemichannels. Ann. Neurol. 57, 749–754.

Lupski, J.R., Garcia, C.A., 2001. Charcot–Marie–Tooth peripheral neuropathies and related disorders. In: Scriver, C.R., Beaudet, A.L., Sly, W.S., Valle, D., Childs, B., Kinzler, K.W. (Eds.), The Metabolic and Molecular Basis of Inherited Disease, 8th ed. McGraw-Hill, New York, pp. 5759–5788.

Mambetisaeva, E.T., Gire, V., Evans, W.H., 1999. Multiple connexin expression in peripheral nerve, Schwann cells, and Schwannoma cells. J. Neurosci. Res. 57, 166–175.

Meier, C., Dermietzel, R., Davidson, K.G.V., Yasumura, T., Rash, J.E., 2004. Connexin32-containing gap junctions in Schwann cells at the internodal zone of partial myelin compaction and in Schmidt–Lanterman incisures. J. Neurosci. 24, 3186–3198.

Menichella, D.M., Goodenough, D.A., Sirkowski, E., Scherer, S.S., Paul, D.L., 2003. Connexins are critical for normal myelination in the central nervous system. J. Neurosci. 23, 5963–5973.

Messing, A., Behringer, R.R., Hammang, J.P., Palmiter, R.D., Brinster, R.L., Lemke, G., 1992. P0 promoter directs expression of reporter and toxin genes to Schwann cells of transgenic mice. Neuron 8, 507–520.

Miyamoto, T., Morita, K., Takemoto, D., Takeuchi, K., Kitano, Y., Miyakawa, T., Nakayama, K., Okamura, Y., Sasaki, H., Miyachi, Y., Furuse, M., Tsukita, S., 2005. Tight junctions in Schwann cells of peripheral myelinated axons: a lesson from claudin-19-deficient mice. J. Cell Biol. 169, 527–538.

Mizisin, A.P., Powell, H.C., 1993. Schwann cell injury is attenuated by aldose reductase inhibition in galactose intoxication. J. Neuropathol. Exp. Neurol. 52, 78–86.

Mizisin, A.P., Shelton, G.D., Wagner, S., Rusbridge, C., Powell, H.C., 1998. Myelin splitting, Schwann cell injury and demyelination in feline diabetic neuropathy. Acta Neuropathol. 95, 171–174.

Musil, L.S., Goodenough, D.A., 1993. Multisubunit assembly of an integral plasma membrane channel protein, gap junction connexin43, occurs after exit from the ER. Cell 74, 1075–1077.

Myers, R.R., Mizisin, A.P., Powell, H.C., Lampert, P.W., 1982. Reduced blood flow in hexachlorophene neuropathy—Relationship to elevated endoneurial fluid pressure. J. Neuropathol. Exp. Neurol. 41, 391–399.

Nelles, E., Butzler, C., Jung, D., Temme, A., Gabriel, H.-D., Dahl, U., Traub, O., Stumpel, F., Jungermann, K., Zielasek, J., Toyka, K.V., Dermietzel, R., Willecke, K., 1996. Defective propagation of signals generated by sympathetic nerve stimulation in the liver of connexin32-deficient mice. Proc. Natl. Acad. Sci. U. S. A. 93, 9565–9570.

Notterpek, L., Shooter, E.M., Snipes, G.J., 1997. Upregulation of the endosomal–lysosomal pathway in the Trembler-J neuropathy. J. Neurosci. 17, 4190–4200.

Odermatt, B., Wellershaus, K., Wallraff, A., Seifert, G., Degen, G., Euwens, C., Fuss, B., Bussow, H., Schilling, K., Stenhauser, C., Willecke, K., 2003. Connexin 47 (Cx47)-deficient mice with enhanced green fluorescent protein reporter gene reveal predominant oligodendrocytic expression of Cx47 and display vacuolized myelin in the CNS. J. Neurosci. 23, 4549–4559.

Palmiter, R.D., Sandgren, E.P., Avarbock, M.R., Allen, D.D., Brinster, R.L., 1991. Heterologous introns can enhance expression of transgenes in mice. Proc. Natl. Acad. Sci. U. S. A. 88, 478–482.

Paulson, H., Garbern, J.Y., Hoban, T.F., Krajewski, K.M., Lewis, R.A., Fischbeck, K.H., Grossman, R.I., Lenkiski, R., Kamholz, J.A., Shy, M.E., 2002. Transient CNS white matter abnormality in X-linked Charcot–Marie–Tooth disease. Ann. Neurol. 52, 429–434.

Paznekas, W.A., Boyadjiev, S.A., Shapiro, R.E., Daniels, O., Wollnik, B., Keegan, C.E., Innis, J.W., Dinulos, M.B., Christian, C., Hannibal, M.C., Jabs, E.W., 2003. Connexin 43 (GJA1) mutations cause the pleiotropic phenotype of oculodentodigital dysplasia. Am. J. Hum. Genet. 72, 408–418.

Pedraza, L., Owens, G.C., Green, L.A.D., Salzer, J.L., 1990. The myelin-associated glycoproteins: membrane disposition, evidence of a novel disulfide linkage between immunoglobulin-like domains, and posttranslational palmitylation. J. Cell Biol. 111, 2651–2661.

Pot, C., Simonen, M., Weinmann, O., Schnell, L., Christ, F., Stoeckle, S., Berger, P., Rulicke, T., Suter, U., Schwab, M.E., 2002. Nogo-A expressed in Schwann cells impairs axonal regeneration after peripheral nerve injury. J. Cell Biol. 159, 29–35.

Richardson, R.R., Donnai, D., Meire, F., Dixon, M.J., 2004. Expression of Gja1 correlates with the phenotype observed in oculodentodigital syndrome/type III syndactyly. J. Med. Genet. 41, 60–67.

Satake, M., Yoshimura, T., Ohnishi, A., Kobayashi, T., 1997. Connexin32 gene expression in rat sciatic nerves and cultured Schwann cells. Dev. Neurosci. 19, 189–195.

Scherer, S.S., Deschênes, S.M., Xu, Y.-T., Grinspan, J.B., Fischbeck, K.H., Paul, D.L., 1995. Connexin32 is a myelin-related protein in the PNS and CNS. J. Neurosci. 15, 8281–8294.

Scherer, S.S., Xu, Y.-T., Nelles, E., Fischbeck, K., Willecke, K., Bone, L.J., 1998. Connexin32-null mice develop a demyelinating peripheral neuropathy. Glia 24, 8–20.

Scherer, S.S., Xu, Y.-T., Messing, A., Willecke, K., Fischbeck, K.H., Bone Jeng, L.J., 2005. Transgenic expression of human Connexin32 in myelinating Schwann cells prevents demyelination in connexin32-null mice. J. Neurosci. 25, 1550–1559.

Shapiro, L., Doyle, J.P., Hensley, P., Colman, D.R., Hendrickson, W.A., 1996. Crystal structure of the extracellular domain from P0, the major structural protein of peripheral nerve myelin. Neuron 17, 435–449.

Shy, M.E., Lupski, J.R., Chance, P.F., Klein, C.J., Dyck, P.J., 2005. Hereditary motor and sensory neuropathies: an overview of clinical, genetic, electrophysiologic, and pathologic features. In: Dyck, P.J., Thomas, P.K., Eds. Peripheral Neuropathy, vol. 2, 4th ed. Saunders, Philadelphia, pp. 1623–1658.

Smit, J.J.M., Bass, F., Hoogendijk, J.E., Jansen, G.H., Vandervalk, M.A., Schinkel, A.H., Berns, A.J.M., Acton, D., Nooter, K., Burger, H., Smith, S.J., Borst, P., 1996. Peripheral neuropathy in mice transgenic for a human MDR3 P-glycoprotein mini-gene. J. Neurosci. 16, 6386–6393.

Söhl, G., Eiberger, J., Jung, Y.T., Kozak, C.A., Willecke, K., 2001. The mouse gap junction gene connexin29 is highly expressed in sciatic nerve and regulated during brain development. Biol. Chem. 382, 973–978.

Taketo, M., Schroeder, A.C., Mobraaten, L.E., Gunning, K.B., Hanten, G., Fox, R.R., Roderick, T.H., Stewart, C.L., Lilly, F., Hansen, C.T., Overbeek, P.A., 1991. FVB/N: an inbred mouse strain preferable for transgenic analyses. Proc. Natl. Acad. Sci. U. S. A. 88, 2065–2069.

Taylor, R.A., Simon, E.M., Marks, H.G., Scherer, S.S., 2003. The CNS phenotype of X-linked Charcot–Marie–Tooth disease: more than a peripheral problem. Neurology 61, 1475–1478.

Tonkin, E.G., Erve, J.C.L., Valentine, W.M., 2000. Disulfiram produces a non-carbon disulfide-dependent Schwannopathy in the rat. J. Neuropathol. Exp. Neurol. 59, 786–797.

Trapp, B.D., Quarles, R.H., 1982. Presence of the myelin-associated glycoprotein correlates with alterations in the periodicity of peripheral myelin. J. Cell Biol. 92, 877–882.

Uhlenberg, B., Schuelke, M., Ruschendorf, F., Ruf, N., Kaindl, A.M., Henneke, M., Thiele, H., StoltenburgDidinger, G., Aksu, F., Topaloglu, H., Nurnberg, P., Hubner, C., Weschke, B., Gartner, J., 2004. Mutations in the gene encoding gap junction protein alpha 12 (Connexin 46.6) cause Pelizaeus–Merzbacher-like disease. Am. J. Hum. Genet. 75, 251–260.

Wang, H.-L., Chang, W.-T., Yeh, T.-H., Wu, T., Chen, M.-S., Wu, C.-Y., 2004. Functional analysis of mutant connexin-32 associated with X-linked dominant Charcot–Marie–Tooth disease. Neurobiol. Dis. 15, 361–370.

White, T.W., 2002. Unique and redundant connexin contributions to lens development. Science 295, 319–320.

Wilson, I.A., Niman, H.L., Houghten, R.A., Cherenson, A.R., Connoly, M.L., Lerner, R.A., 1984. The structure of an antigenic determinant in a protein. Cell 37, 767–778.

Wrabetz, L., Feltri, M.L., Kleopa, K.A., Scherer, S.S., 2004. Inherited neuropathies—Clinical, genetic, and biological features. In: Lazzarini, R.A. (Ed.), Myelin Biology and Disorders, vol. 2. Elsevier, San Diego, pp. 905–951.

Yin, X., Peterson, J., Gravel, M., Braun, P.E., Trapp, B.D., 1997. CNP overexpression induces aberrant oligodendrocyte membranes and inhibits MBP accumulation and myelin compaction. J. Neurosci. Res. 50, 238–247.

Yoshimura, T., Satake, M., Kobayashi, T., 1996. Connexin43 is another gap junction protein in the peripheral nervous system. J. Neurochem. 67, 1252–1258.

Yum, S.W., Kleopa, K.A., Shumas, S., Scherer, S.S., 2002. Diverse trafficking abnormalities for connexin32 mutants causing CMTX. Neurobiol. Dis. 11, 43–52.

Zhao, S., Spray, S., 1998. Localization of Cx26, Cx32 and Cx43 in myelinating Schwann cells of mouse sciatic nerve during postnatal development. In: Werner, R. (Ed.), Gap Junctions. IOS Press, Amsterdam, pp. 198–202.